KIAS-P10048

Unusual Higgs boson signal in R-parity violating nonminimal supersymmetric models at the LHC

Priyotosh Bandyopadhyay*,[1,†] Pradipta Ghosh,[2,‡] and Sourov Roy[2,§]

[1] *Korea Institute for Advanced Study, Hoegiro 87 (207-43 Cheongnyangni-dong), Seoul 130-722, Korea*
[2] *Department of Theoretical Physics, Indian Association for the Cultivation of Science, 2A and 2B Raja S.C. Mullick Road, Kolkata 700 032, India*

We predict an unconventional background free signal of the Higgs boson in R-parity violating nonminimal supersymmetric models at the Large Hadron Collider (LHC). The signal comprises dilepton plus four hadronic jets and two large displaced vertices. The displaced leptons and jets are coming from the decay of the lightest supersymmetric particle (LSP), which is predominantly a gauge-singlet neutrino. A pair of such LSPs can couple to a Higgs boson, created via gluon fusion. We have analyzed two cases - one corresponding to the tree-level Higgs boson mass and another with the one-loop corrected mass of the Higgs boson. A reliable Higgs mass reconstruction using this signal can lead to discovery at the LHC with center-of-mass energy $\sqrt{s} = 14$ TeV and 5 fb^{-1} of integrated luminosity ($\mathcal{L}$). Even at $\sqrt{s} = 7$ TeV and $\mathcal{L} = 5$ fb^{-1}, a reasonable number of events are expected. Besides, mass reconstruction of a gauge-singlet LSP can provide an estimate of the seesaw scale.

PACS numbers: 12.60.Jv, 14.60.Pq, 14.60.St, 14.80.Da

I. INTRODUCTION

Supersymmetric theories have commendable success in taming the ill behaved quadratic divergences of the mass of the hitherto unseen standard model (SM) Higgs boson. Recently, inception of the LHC experiment at CERN has given fresh impetus to the hope of discovering the Higgs boson and weak scale supersymmetry.

In this paper, we propose a prodigious signal for the Higgs boson in supersymmetry, having a pair of leptons and four hadronic jets along with large displaced vertices ($\gtrsim 2$ m). With the aid of these displaced vertices, all of the SM backgrounds can be effaced. Displaced vertices arising from minimal supersymmetric standard model (MSSM) with R_p violation ($\not{R}_p$) (see review [1]) are usually much smaller [2], and thus hardly mimic this signal. Furthermore, the imprint of this signal is different from that of the cosmic muons which have definite entry and exit point in the detector. So this is apparently a clean signal and a discovery, thus, is definite even with small number of signal events.

This unusual signal would produce visible tracks in the muon chamber of the CMS or ATLAS detector (electrons will be absorbed in the iron yoke of muon-chamber), along with some accompanying noise (from the associated hadronic jets). These tracks are isolated tracks produced by stand-alone muons without any matching tracks in the inner detector. It is indeed difficult for the conventional triggers to work for this specific signal; rather this asks for a dedicated special trigger which we believe is a challenging task for experimentalists. Nevertheless, in addition to this final state topology, one can also have the usual global muon signatures which produce continuous matching tracks in the detector, starting from the inner tracker to the muon chamber, but with smaller displaced vertices. The associated electrons and hadronic jets also leave their signatures in the inner tracker and calorimeters. These events can be easily triggered with conventional triggers.

II. THE MODEL

The underlying model contains $\not{R}_p$ and, is nonminimal in nature with SM gauge singlet right-handed neutrino superfields ($\hat{\nu}_i^c$). The right sneutrinos ($\widetilde{\nu}_i^c$) through their vacuum expectation values provide a solution [3, 4] to the μ-problem [5]. Besides, the right-handed neutrinos (ν_i^c) together with $\not{R}_p$ are instrumental for light neutrino mass generation [6–9], consistent with three flavour global fit [10]. This model

*Present address: Helsinki Institute of Physics and Helsinki University Gustaf Hällströmin Katu 2, POB-64, FIN-00014, Helsinki, Finland.
†Electronic address: priyotosh.bandyopadhyay@helsinki.fi
‡Electronic address: tppg@iacs.res.in
§Electronic address: tpsr@iacs.res.in

is known as the $\mu\nu$SSM [3, 4].

The superpotential of $\mu\nu$SSM is given by,

$$W = W' + \epsilon_{ab} Y_\nu^{ij} \hat{H}_u^b \hat{L}_i^a \hat{\nu}_j^c - \epsilon_{ab} \lambda^i \hat{\nu}_i^c \hat{H}_d^a \hat{H}_u^b + \frac{1}{3} \kappa^{ijk} \hat{\nu}_i^c \hat{\nu}_j^c \hat{\nu}_k^c, \quad (1)$$

where W' is the MSSM superpotential without the μ-term. Lepton number violation (Ł) by odd unit(s) in the last two terms of Eq.(1) triggers $\not{R}_p$. The fourth term of Eq.(1) apart from excluding the massless axion [11], generates TeV scale right-chiral neutrino *Majorana* masses. Bilinear terms are forbidden in W by an imposed Z_3 symmetry. The associated problem of domain wall formation [12] from spontaneous breaking of this Z_3 symmetry can be ameliorated through known methods [13]. Scalar and fermion sectors for $\mu\nu$SSM are addressed in Refs. [4, 6, 7, 9].

The neutralino LSP, $\widetilde{\chi}_1^0$ in $\mu\nu$SSM can be predominantly ($\gtrsim 70\%$) ν^c-like (also known as a *singlino* LSP). $\widetilde{\chi}_1^0$ being singlet, $\widetilde{\chi}_1^0\widetilde{\chi}_1^0 Z$ or $\widetilde{\chi}_1^0 q\widetilde{q}$ couplings [9] are vanishingly small, which in turn results in very small cross-section for direct $\widetilde{\chi}_1^0$ pair production. On the contrary, the third term of Eq.(1) may produce a large $\widetilde{\chi}_1^0\widetilde{\chi}_1^0 S_i^0$ [9] coupling with $\lambda \sim \mathcal{O}$ (1), where S_i^0 are the scalar states. With the chosen set of parameters (see Table I) we obtained $S_4^0 \equiv h^0$, where h^0 is the lightest Higgs boson of MSSM. In addition, with heavy squark/gluino masses as indicated in Table I for different benchmark points, production of a singlino LSP through cascade decays is suppressed. In the backdrop of such a scenario, production of h^0 in the gluon fusion channel followed by the decay process $h^0 \to \widetilde{\chi}_1^0\widetilde{\chi}_1^0$ will be the leading production channel for the singlino LSP at the LHC. We want to emphasize here that for the first part of our analysis we choose to work with the tree level mass of the lightest CP-even Higgs boson ($S_4^0 \equiv h^0$) of the $\mu\nu$SSM. With loop corrections the Higgs boson mass can be much higher [4, 7]. For loop corrected Higgs boson mass, the process $h^0 \to \widetilde{\chi}_1^0\widetilde{\chi}_1^0$ can produce heavy singlinolike LSPs with smaller decay lengths [7]. However, our general conclusions will not change for a singlino LSP in the mass range $40 - 60$ GeV. We will present a similar analysis with the one-loop correction in the neutral scalar sector in detail, to justify our statement.

III. SCENARIO-I

In this section we present a detailed analysis of the unconventional signal mentioned in the introduction, with the tree level mass spectra of $\mu\nu$SSM. A set of four benchmark points (BPs) used for collider studies compatible with neutrino data [10], up to one-loop level analysis of neutrino masses, and mixing [9] are given in Table I. Here we have shown the physical mass spectra and the values of only two parameters, namely, μ and $\tan\beta$. Other parameters are not shown here. However, note that these are sample points and similar spectra can be obtained in a reasonably large region of the parameter space even after satisfying all the constraints from neutrino experiments.

TABLE I: μ-parameter, tanβ and relevant mass spectrum (GeV) for the chosen benchmark points. $m_{\widetilde{\chi}_{1,2,3}^\pm} \equiv m_{e,\mu,\tau}$.

	BP-1	BP-2	BP-3	BP-4
μ	177.0	196.68	153.43	149.12
$\tan\beta$	10	10	30	30
m_{h^0} ($\equiv m_{S_4^0}$)	91.21	91.63	92.74	92.83
$m_{S_1^0}$	48.58	49.33	47.27	49.84
$m_{P_2^0}$	47.21	49.60	59.05	49.45
$m_{S_2^\pm}$	187.11	187.10	187.21	187.21
$m_{\tilde{b}_1}$	831.35	831.33	830.67	830.72
$m_{\tilde{b}_2}$	875.03	875.05	875.72	875.67
$m_{\tilde{t}_1}$	763.41	763.63	761.99	761.98
$m_{\tilde{t}_2}$	961.38	961.21	962.46	962.48
$m_{\widetilde{\chi}_1^0}$	43.0	44.07	44.20	44.24
$m_{\widetilde{\chi}_2^0}$	55.70	57.64	61.17	60.49
$m_{\widetilde{\chi}_4^\pm}$	151.55	166.61	133.69	130.77

For the set of specified benchmark points, we observe, the process $h^0 \to \widetilde{\chi}_1^0\widetilde{\chi}_1^0$ to be one of the dominant decay modes of h^0 (branching fraction within 35-65%), while the process $h^0 \to b\bar{b}$ remains the main competitor. In Table I only the third generation squark masses are shown.

The mass of $\widetilde{\chi}_1^0$ ($m_{\widetilde{\chi}_1^0}$) for the chosen points is always less than m_W (see Table I). For such a light $\widetilde{\chi}_1^0$, at the tree level only three body decay modes are allowed. General three body final states are,

$$\widetilde{\chi}_1^0 \to b\bar{b}\nu_k,\ \ell_i^+\ell_j^-\nu_k,\ q_i\bar{q}_i\nu_k,\ q_i\bar{q}_j'\ell_k^\mp,\ \nu_i\bar{\nu}_j\nu_k, \quad (2)$$

where i, j, k are flavor indices. We choose the specific decay mode $\widetilde{\chi}_1^0 \to q_i\bar{q}_j'\ell_k^\pm$ to yield a signal $pp \to 2\ell + 4j + X$ in the final state. The dilepton have same sign on 50% occurrence since $\widetilde{\chi}_1^0$ is a Majorana particle. Detection of these leptons and jets can lead to reliable mass reconstruction for $\widetilde{\chi}_1^0$ and Higgs boson in the absence of missing energy in the final state. There is one more merit of this analysis; i.e., invariant mass reconstruction for a singlino LSP can give us an estimation of the seesaw scale, since the right-handed neutrinos are operational in light neutrino mass generation through a TeV scale seesaw mechanism [3, 6].

For the chosen benchmark points $Br(\widetilde{\chi}_1^0 \to q_i \bar{q}'_j \ell_k^{\pm})$ lies within $8-10\%$. However, concerning the real experimental ambience, extra jets can arise from initial state radiation and final state radiation. Likewise semileptonic decays of quarks can accrue extra leptons. Also from the experimental point of view one cannot have zero missing p_T in the final state. With this set of information we optimize our chosen signal as

$$(n_j \geq 4) + (n_\ell \geq 2) + (\not{p}_T \leq 30 \text{ GeV}), \qquad (3)$$

where $n_{j(\ell)}$ represents the number of *jets(leptons)*.

It should be noted that, similar final states can appear from the decay of heavier scalar or pseudoscalar states in the model. Obviously, their production cross section will be smaller compared to h^0 and the invariant mass distribution (some other distributions also) should be different in those cases.

`PYTHIA (version 6.4.22) [14]` has been used for the purpose of event generation. The corresponding mass spectrum and decay branching fractions are fed to `PYTHIA` by using the SLHA interface [15]. Subsequent decays of the produced particles, hadronization and the collider analysis were performed using `PYTHIA`. We used `CTEQ5L` parton distribution function (PDF) [16] for the analysis. The renormalization/factorization scale Q was chosen to be the parton level center-of-mass energy, $\sqrt{\hat{s}}$. We also kept initial state radiation, final state radiation and multiple interaction on for the analysis. The production cross-section of h^0 via gluon fusion channel for different benchmark points (Table I) is shown in Table II.

TABLE II: Hard scattering cross-section in fb for the process $gg \to h^0$ for PDF CTEQ5L with $Q = \sqrt{\hat{s}}$.

	BP-1	BP-2	BP-3	BP-4
$\sqrt{s} = 7$ TeV	6837	7365	6932	6948
$\sqrt{s} = 14$ TeV	23150	25000	23580	23560

We have used `PYCELL`, the toy calorimeter simulation provided in `PYTHIA`, with the following criteria:
I. The calorimeter coverage is $|\eta| < 4.5$ and the segmentation is given by $\Delta\eta \times \Delta\phi = 0.09 \times 0.09$ which resembles a generic LHC detector.
II. $\Delta R \equiv \sqrt{(\Delta\eta)^2 + (\Delta\phi)^2} = 0.5$ has been used in cone algorithm for jet finding.
III. $p_{T,min}^{jet} = 10$ GeV.
IV. No jet matches with a hard lepton in the event.

In addition, the following set of standard kinematic cuts were incorporated throughout:

1. $p_T^\ell \geq 5$ GeV and $|\eta|_\ell \leq 2.5$,
2. $|\eta|_j \leq 2.5$, $\Delta R_{\ell j} \geq 0.4$, $\Delta R_{\ell\ell} \geq 0.2$,

where $\Delta R_{\ell j}$ and $\Delta R_{\ell\ell}$ measure the lepton-jet and lepton-lepton isolation, respectively. Events with isolated leptons, having $p_T \geq 5$ GeV are taken for the final state analysis.

One of the striking features in $\mu\nu$SSM is that certain ratios of branching fractions of the LSP decay modes are correlated with the neutrino mixing angles [6, 7]. This implies $n_\mu > n_e$ in the final state. Fig.1 shows the lepton multiplicity distribution for inclusive $\geq 2\ell$ ($\geq 2\mu + \geq 2e + 1\mu, 1e$) and exclusive ($\geq 2\mu, \geq 2e$) for BP-2, without the signal criteria [Eq.(3)]. Muon dominance of the higher histograms (without any isolation cuts) continues to the lower ones even after the application of $\Delta R_{\ell j}$, $\Delta R_{\ell\ell}$ cuts. Consequently, we observe that the correlation between n_e and n_μ also appears in the lower histograms (Fig.1) with a ratio $\sim$ 1:3.

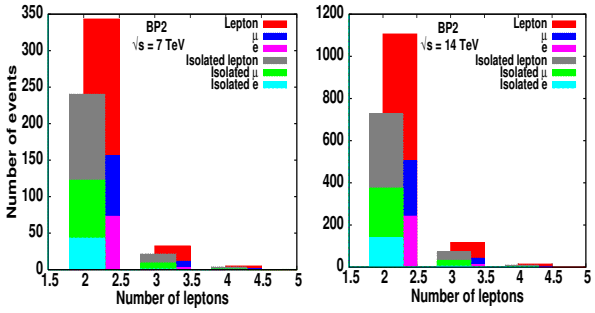

FIG. 1: Lepton multiplicity distribution of signal for $\sqrt{s} =$ 7 and 14 TeV with 1 fb^{-1} of integrated luminosity. For more details, see text.

We present number of events for final state signal (Eq. 3) in Table III both for $\sqrt{s} = 7$ and 14 TeV for $\mathcal{L} = 5$ fb^{-1}, without a cut on the actual $\widetilde{\chi}_1^0$ decay position. The average decay length for a singlinolike LSP is determined by the LSP mass as well as by a set of parameters $(\lambda, \kappa, v^c, Y_\nu^{ii}, v'_i)$ so that the constraints on neutrino masses and mixing are satisfied. Here v^c and v'_i stand for the vacuum expectation values of the right- and left-handed sneutrino fields. The average decay length increases for smaller LSP mass and for a singlinolike LSP with a mass ~ 20 GeV, the average decay length comes out to be ~ 100 meters [7]. For such a choice, a large fraction of the LSPs will decay outside the detector. We have not considered such possibilities in our analysis. The average decay lengths for all the four benchmark points are shown in Table IV. It is interesting to note from Table III that the correlation between n_e and n_μ in the final state is still well maintained, similar to what was shown in

the lower histograms of Fig.1 even with the final state signal topology [Eq.(3)].

TABLE III: Expected number of events of signals for $\mathcal{L} = 5$ fb^{-1} for $\sqrt{s} = 7$ and 14 TeV.

$\sqrt{s}$	signal	BP-1	BP-2	BP-3	BP-4
7 TeV	$\geq 4j + \geq 2\ell + \not{p}_T \leq 30$ GeV	181	153	170	173
	$\geq 4j + \geq 2\mu + \not{p}_T \leq 30$ GeV	100	85	97	100
	$\geq 4j + \geq 2e + \not{p}_T \leq 30$ GeV	27	23	21	23
	$\geq 4j + 1e + 1\mu + \not{p}_T \leq 30$ GeV	54	46	52	50
14 TeV	$\geq 4j + \geq 2\ell + \not{p}_T \leq 30$ GeV	1043	878	951	929
	$\geq 4j + \geq 2\mu + \not{p}_T \leq 30$ GeV	580	463	533	513
	$\geq 4j + \geq 2e + \not{p}_T \leq 30$ GeV	160	139	121	129
	$\geq 4j + +1e + 1\mu + \not{p}_T \leq 30$ GeV	306	279	300	290

TABLE IV: Average decay lengths (L) for a singlino LSP for different benchmark points.

	BP-1	BP-2	BP-3	BP-4
L (meter)	5.20	4.23	5.20	5.35

The entries of Table III suffer a diminution with a cut on the $\widetilde{\chi}_1^0$ decay position. Table V represents the number of signal events in different ranges of the transverse decay length (L_T) for BP-2, after applying the cuts. Other benchmark points show similar behaviour. The number of events with decay length (see Table V) near the muon chamber at CMS is approximately $\sim$ 10% of the total number of events. However, being free of backgrounds even this can lead

TABLE V: Number of signal events for $\mathcal{L} = 5$ fb^{-1} for $\sqrt{s} = 7$ and 14 TeV at different ranges of the decay length for BP-2 with 1 $cm < L_{T_1} \leq 50$ cm, 50 $cm < L_{T_2} \leq 3$ m and 3 $m < L_{T_3} \leq 6$ m. L_{T_i}s are different transverse decay lengths.

		No. of events		
$\sqrt{s}$	signal	L_{T_1}	L_{T_2}	L_{T_3}
7 TeV	$\geq 4j + \geq 2\ell + \not{p}_T \leq 30$ GeV	45	69	17
	$\geq 4j + \geq 2\mu + \not{p}_T \leq 30$ GeV	27	38	11
	$\geq 4j + \geq 2e + \not{p}_T \leq 30$ GeV	6	10	2
	$\geq 4j + 1e + 1\mu + \not{p}_T \leq 30$ GeV	12	21	4
14 TeV	$\geq 4j + \geq 2\ell + \not{p}_T \leq 30$ GeV	234	373	98
	$\geq 4j + \geq 2\mu + \not{p}_T \leq 30$ GeV	128	218	58
	$\geq 4j + \geq 2e + \not{p}_T \leq 30$ GeV	37	45	16
	$\geq 4j + +1e + 1\mu + \not{p}_T \leq 30$ GeV	69	113	24

to discovery at 14 TeV run of the LHC with $\mathcal{L} = 5$ fb^{-1}. At 7 TeV the situation looks much less promising and much higher luminosity is required for discovering such an event. There exists reasonable number of events ($\sim$ 30%) with decay length in between 1 cm and 50 cm (see Table V and Fig.2). As stated earlier these events can leave their signs in inner tracker and calorimeters as well as can produce tracks in the muon chamber. Besides, about $\sim$ 40% of signal events appear in the range of 50 cm to 3 m which may or may not leave traces in tracker and calorimeters depending on the decay length but will definitely produce visible tracks in the muon chamber. Thus we can have novel final states observed not only in the muon chambers of the LHC detectors but also in the inner tracker and calorimeters. Therefore combining these different signatures new discoveries are envisaged. A very small fraction of events ($\sim$ 4%) do have a decay length greater than the size of the CMS detector (For ATLAS this fraction is somewhat smaller) which will yield the conventional missing energy signature.

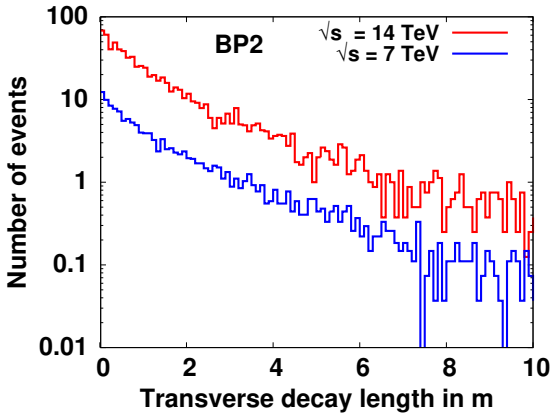

FIG. 2: Transverse decay length distribution of $\widetilde{\chi}_1^0$ for $\sqrt{s} = 7$ and 14 TeV with BP-2 for a typical detector size ~ 10 m with $\mathcal{L} = 5$ fb^{-1}. Minimum bin size is 10 cm. The signal is given by Eq.(3).

Results of invariant mass reconstruction for $\widetilde{\chi}_1^0$ and h^0 for BP-2 are shown in Fig.3. We choose $jj\ell$ invariant mass $M(jj\ell)$ for $m_{\widetilde{\chi}_1^0}$ reconstruction. Reconstruction of m_{h^0} was achieved through $M(jjjj\ell\ell)$, invariant mass of $jjjj\ell\ell$ [see Eq.(3)]. We take the jets and leptons from the window of 35 GeV $\leq$ M(jjℓ) $\leq$ 45 GeV to construct $M(jjjj\ell\ell)$. Even a narrow window like this cannot kill all the combinatorial backgrounds. As a corollary, effect of combinatorial background for $m_{\widetilde{\chi}_1^0}$ reconstruction ($^4C_2$ for j and $^2C_1$ for ℓ) also causes long tail for Higgs mass distribution.

IV. SCENARIO-II

In this section we present a similar analysis like scenario-I, but with the inclusion of one-loop radiative correction in the neutral scalar sector. Mass of the lightest doubletlike Higgs boson increases as an effect of adding the one-loop correction in the scalar sector and consequently the process $h^0 \to \widetilde{\chi}_1^0\widetilde{\chi}_1^0$ can yield a

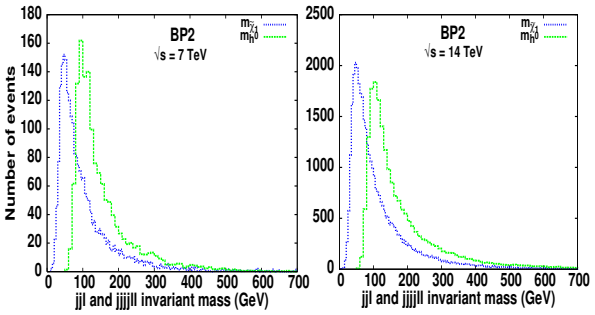

FIG. 3: Invariant mass distribution for $\widetilde{\chi}_1^0$ $(jj\ell)$, as well as the Higgs boson $(jjjj\ell\ell)$. Plots are shown for $\sqrt{s} = 7$ and 14 TeV with 1 fb^{-1} of integrated luminosity. The Number of events for reconstructing $m_{\widetilde{\chi}_1^0}$ for $\sqrt{s} = 7(14)$ TeV are scaled by a multiplicative factor 4(7).

heavier singlinolike LSP, compared to the benchmark points presented in Table I. Also a heavier singlino LSP will give rise to a smaller decay length and thus offer a better chance of detecting this unusual signal at a collider experiments. All of these features will be explored in further details in the subsequent paragraphs. For the one-loop corrections to the neutral scalar sector of the $\mu\nu$SSM we consider the dominant contributions only, coming from the quarks and squarks in the loop[4]. The A_0 and B_0 functions [17, 18] appearing in the loop calculations are chosen according to Ref. [19]. A set of two benchmark points with one-loop corrected neutral scalar masses are shown in Table VI.

TABLE VI: μ-parameter, tanβ and relevant mass spectrum (GeV) for benchmark points with one-loop corrected scalar masses. $m_{\widetilde{\chi}_{1,2,3}^{\pm}} \equiv m_{e,\mu,\tau}$ and $m_{h^0} \equiv m_{S_4^0}$.

	BP-5	BP-6
μ	137.19	145.08
tanβ	30	10
m_{h^0}	115.01	119.36
$m_{S_1^0}$	61.11	61.07
$m_{S_2^0}$	61.11	61.07
$m_{S_3^0}$	61.21	62.25
$m_{P_2^0}$	69.87	66.59
$m_{S_2^{\pm}}$	187.22	187.12
$m_{\widetilde{b}_1}$	830.85	831.37
$m_{\widetilde{b}_2}$	875.55	875.00
$m_{\widetilde{t}_1}$	761.93	763.06
$m_{\widetilde{t}_2}$	962.51	961.66
$m_{\widetilde{\chi}_1^0}$	52.72	54.60
$m_{\widetilde{\chi}_2^0}$	73.71	74.90
$m_{\widetilde{\chi}_4^{\pm}}$	120.85	125.53

Since we consider effect of one-loop corrections only to the neutral scalar sector and not for the neutral pseudoscalar sector, for these set of benchmark points neutrino data [10] are satisfied only for tree level neutrino masses and mixing. A complete analysis of one-loop corrected neutrino masses and mixing with scalar as well as pseudoscalar Higgs boson masses at the one-loop level is beyond the scope of the present paper. The trilinear couplings A_u and A_d have been chosen accordingly [4], in order to obtain different mass eigenvalues of the lightest doubletlike neutral Higgs boson. Another important observation with the inclusion of one-loop radiative corrections to the scalar sector of $\mu\nu$SSM is that for the doubletlike Higgs ($h^0 \equiv S_4^0$) the following two body decays $h^0 \to S_i^0 S_j^0, P_a^0 P_b^0$ with $i, j = 1, 2, 3$ and $a, b = 2, 3, 4$ become kinematically more accessible. Thus unlike $h^0 \to b\bar{b}$ for scenario-I, these processes can now become the dominant competitors to achieve a reasonable branching ratio for the process $h^0 \to \widetilde{\chi}_1^0 \widetilde{\chi}_1^0$. However, in the present analysis we have avoided such a situation. A pair of benchmark points has been chosen such that the two-body decays like $h^0 \to S_i^0 S_j^0, P_a^0 P_b^0$ are kinematically disfavoured. These are presented in Table VI. For these benchmark points (BP5 and BP6), the process $h^0 \to b\bar{b}$ remains the main competitor to achieve a large $Br(h^0 \to \widetilde{\chi}_1^0 \widetilde{\chi}_1^0)$. Three body decays of h^0 into $Zf\bar{f}$ or $W^{\pm} f_1 f_2$ (where f, f_1, f_2 are either leptons or quarks) share very small branching ratios [7] when two body decays are kinematically allowed. For the two benchmark points shown in Table VI the singlino purity is set to be $\gtrsim 60\%$.

As argued earlier, with one-loop corrected Higgs boson mass, the process $h^0 \to \widetilde{\chi}_1^0 \widetilde{\chi}_1^0$ can yield heavy singlinolike LSPs with smaller decay lengths which are shown in Table VII. It is clear from Table VII, that for $m_{\widetilde{\chi}_1^0} \sim 50 - 55$ GeV, the decay lengths are $\sim \mathcal{O}$ $(2 - 2.5$ m). The singlino LSP mass as shown in Table VI are higher compared to those shown in Table I. In general, the average decay length can vary from $2 - 8$ m depending on the LSP mass in the range of $40 - 55$ GeV. It is to be noted that unlike scenario-I, here the branching ratio for the process $h^0 \to \widetilde{\chi}_1^0 \widetilde{\chi}_1^0$ lies within $45\% - 85\%$, whereas $Br(\widetilde{\chi}_1^0 \to q_i \bar{q}'_j \ell_k^{\pm})$ lies in the same range as in scenario-I.

As discussed earlier, even lighter singlinolike LSP ($m_{\widetilde{\chi}_1^0} \sim 20$ GeV) can be achieved with smaller values of the trilinear coupling κ in the superpotential. However, the associated average decay length will be very large $\sim \mathcal{O}$ (100) m [7] and a large fraction of the LSPs will decay outside the detector. In addition to a very large decay length, smaller κ values will make decays like $h^0 \to S_i^0 S_j^0, P_a^0 P_b^0$ kinematically

possible, with lighter scalar and pseudoscalar states. These decays, when allowed are usually the dominant decay modes for h^0 which lead to the different final state. Thus, combining the two scenarios (with tree-level and one-loop corrected Higgs boson mass), we conclude that the discovery of the signal discussed in this paper works in the range of LSP mass $\sim$ 40-60 GeV.

TABLE VII: Average decay lengths (L) for a singlino LSP for different benchmark points with one-loop corrected scalar masses.

	BP-5	BP-6
L (meter)	2.65	2.10

The approach of collider analysis is exactly the same as that of scenario-I. The production cross-section of one-loop corrected h^0 via gluon fusion channel for different benchmark points (Table VI) is given in Table VIII. It is evident from Table II and Table VIII that the hard scattering cross-section for h^0 production through gluon fusion at the LHC suffers diminution with the inclusion of one-loop radiative corrections.

TABLE VIII: Hard scattering cross-section in fb for the process $gg \to h^0$ for PDF CTEQ5L with $Q = \sqrt{\hat{s}}$ with one-loop corrected scalar masses.

	BP-5	BP-6
$\sqrt{s} = 7$ TeV	4211.04	3759.31
$\sqrt{s} = 14$ TeV	15135.68	13712.05

Also we present the number of signal events with a cut on $\widetilde{\chi}_1^0$ decay position in Table IX for BP-5, which is exactly similar to that of Table V but with one-loop corrected CP-even scalar masses.

TABLE IX: Number of signal events for $\mathcal{L} = 5$ fb^{-1} for $\sqrt{s} = 7$ and 14 TeV at different ranges of the decay length for BP-5 with 1 $cm < L_{T_1} \leq 50$ cm, 50 $cm < L_{T_2} \leq 3$ m and 3 $m < L_{T_3} \leq 6$ m. L_{T_i}s are different transverse decay lengths with one-loop corrected scalar masses.

		No. of events		
$\sqrt{s}$	signal	L_{T_1}	L_{T_2}	L_{T_3}
	$\geq 4j + \geq 2\ell + \not{p}_T \leq 30$ GeV	71	101	15
7	$\geq 4j + \geq 2\mu + \not{p}_T \leq 30$ GeV	45	64	9
TeV	$\geq 4j + \geq 2e + \not{p}_T \leq 30$ GeV	8	11	0.4
	$\geq 4j + 1e + 1\mu + \not{p}_T \leq 30$ GeV	18	26	6
	$\geq 4j + \geq 2\ell + \not{p}_T \leq 30$ GeV	371	523	86
14	$\geq 4j + \geq 2\mu + \not{p}_T \leq 30$ GeV	221	315	52
TeV	$\geq 4j + \geq 2e + \not{p}_T \leq 30$ GeV	50	72	12
	$\geq 4j + +1e + 1\mu + \not{p}_T \leq 30$ GeV	99	138	22

Since the average decay length is smaller for a heavier neutralino originating from the decay of h^0 with one-loop corrected mass, now almost $\sim$ 35% of the total number of events appears within $1 - 50$ cm and roughly $\sim$ 50% of the total number of signal events appears within 50 $cm - 3$ m. Integrating the signatures of this signal in the two above mentioned range of decay lengths, one can observe either tracks in the tracker and calorimeters along with conventional global muon signature (LSP decay length in the range $1 - 50$ cm) or tracks in the muon chamber without matching tracks in the tracker and calorimeters (for LSP decay length close to 3 m). In the case of LSP decay lengths between 50 cm and 2 m, one can have signatures in the electromagnetic calorimeter and/or hadronic calorimeter (depending on the actual decay position) along with the muon tracks in the muon chamber. The fraction of total number of events appearing completely in the muon chamber (LSP decay length between 3 and 6 m) with stand alone muon signature is slightly less ($\sim$ 8%) compared to scenario-I, but still reasonable enough to lead to new discovery particularly with the $\sqrt{s} = 14$ TeV run of LHC.

For the 7 TeV LHC run things are definitely less promising and would require a higher luminosity for claiming discovery. Since the average decay length is small for the two benchmark points studied for scenario-II (see Table VII), the fraction of events appearing outside the detector is $\sim 1 - 2\%$ of the total number of events, which is smaller compared to scenario-I. All of these features are also evident from Fig. 4, where the transverse decay length distribution is shown for BP-5. So once again combining the entire range of LSP decay length, we can have novel final states observed not only in the muon chambers of the LHC detectors but also in the inner tracker and calorimeters. Therefore, with the observation of these different signatures, new discoveries are envisaged even with the inclusion of one-loop corrections in the scalar sector.

Results of invariant mass reconstruction for $\widetilde{\chi}_1^0$ and h^0 for BP-5 are shown in Fig.5 but with $\sqrt{s} = 14$ TeV of LHC run only. As already stated in the context of Fig.3, we choose $jj\ell$ invariant mass $M(jj\ell)$ for $m_{\widetilde{\chi}_1^0}$ reconstruction. This plot is similar to that of Fig.3 with similar explanations.

V. CONCLUSION

In conclusion, we have studied an unusual but spectacular signal of Higgs boson in supersymmetry. This

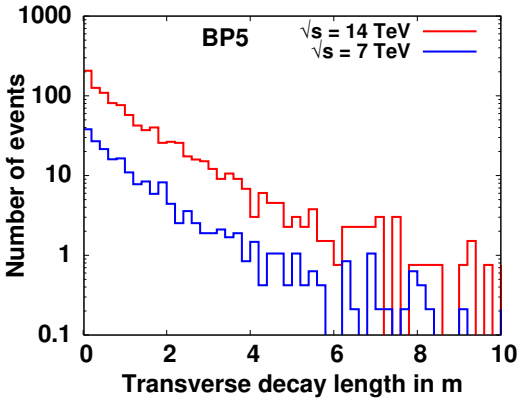

FIG. 4: Transverse decay length distribution of $\widetilde{\chi}_1^0$ for $\sqrt{s} = 7$ and 14 TeV with BP-5 for a typical detector size $\sim 10\ m$ with $\mathcal{L} = 5$ fb^{-1}. Minimum bin size is 20 cm. The signal is given by Eq.(3).

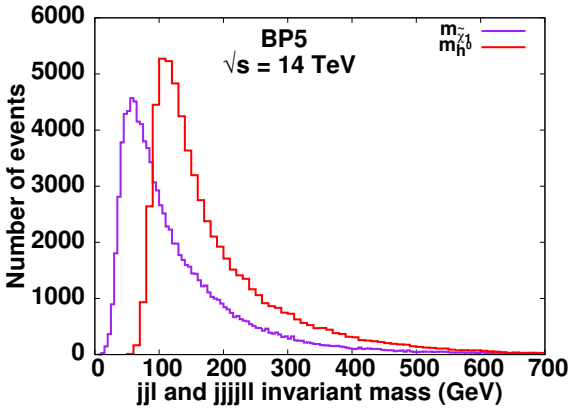

FIG. 5: Invariant mass distribution for $\widetilde{\chi}_1^0$ $(jj\ell)$, as well as the Higgs boson $(jjjj\ell\ell)$. Plot is given for 14 TeV with 5 fb^{-1} of integrated luminosity. The Number of events for reconstructing $m_{\widetilde{\chi}_1^0}$ for $\sqrt{s} = 14$ TeV are scaled by a multiplicative factor 7.

signal can give rise to non-standard activities in the muon chamber with muon(s) and four hadronic jets. There are, however, number of events which can leave their imprints not only at the muon chamber but also in the inner tracker and calorimeters concurrently. Integrating these two signatures can lead to discovery of an unusual signal of Higgs boson at the 14 TeV run of the LHC. Though with higher luminosity, discovery at $\sqrt{s}$ =7 TeV is also possible. Indubitably, developement of new triggers and event reconstruction tools is essential. This signal is generic to a class of models where gauge-singlet neutrinos and $\not{R}_p$ take part simultaneously in generating neutrino masses and mixing. Another interesting feature of this study is that the number of muonic events in the final state is larger than the number of electron events and the ratio of these two numbers can be predicted from the study of the neutrino mixing angles. It is also important to note that such a generic conclusion remains valid with and without considering the effect of one-loop corrections in the scalar sector.

We thank Satyaki Bhattacharya, Manas Maity and Bruce Mellado for very helpful discussions. PB wants to thank KIAS for its "quest" computational facility and overseas travel grant during the project. PG acknowledges the financial support of the CSIR, Government of India.

[1] R. Barbier *et al.*, Phys. Rept. **420** 1(2005).
[2] B. Mukhopadhyaya, S. Roy and F. Vissani, Phys. Lett. B **443**, 191 (1998); S. Y. Choi *et al.*, Phys. Rev. D **60**, 075002 (1999); J. C. Romao *et al.*, Phys. Rev. D **61**, 071703 (2000).
[3] D. E. Lopez-Fogliani and C. Munoz, Phys. Rev. Lett. **97**, 041801 (2006).
[4] N. Escudero, D. E. Lopez-Fogliani, C. Munoz and R. R. de Austri, JHEP **0812**, 099 (2008).
[5] J. E. Kim and H. P. Nilles, Phys. Lett. B **138**, 150 (1984).
[6] P. Ghosh and S. Roy, JHEP **0904**, 069 (2009).
[7] A. Bartl *et al.*, JHEP **0905**, 120 (2009).
[8] J. Fidalgo, D. E. Lopez-Fogliani, C. Munoz and R. Ruiz de Austri, JHEP **0908**, 105 (2009).
[9] P. Ghosh, P. Dey, B. Mukhopadhyaya and S. Roy, JHEP **1005**, 087 (2010).
[10] T. Schwetz, M. A. Tortola and J. W. F. Valle, New J. Phys. **10**, 113011 (2008).
[11] J. R. Ellis *et al.*, Phys. Rev. D **39**, 844 (1989).
[12] J. R. Ellis *et al.*, Phys. Lett. B **176**, 403 (1986); B. Rai and G. Senjanovic, Phys. Rev. D **49**, 2729 (1994); S. A. Abel, S. Sarkar and P. L. White, Nucl. Phys. B **454**, 663 (1995).
[13] S. A. Abel, Nucl. Phys. B **480**, 55 (1996); C. Panagiotakopoulos and K. Tamvakis, Phys. Lett. B **446**, 224 (1999).
[14] T. Sjostrand, S. Mrenna and P. Z. Skands, JHEP **0605**, 026 (2006).
[15] P. Z. Skands *et al.*, JHEP **0407**, 036 (2004).
[16] H. L. Lai *et al.* [CTEQ Collaboration], Eur. Phys. J. C **12**, 375 (2000); J. Pumplin *et al.*, JHEP **0207**, 012

(2002).

[17] G. 't Hooft and M. J. G. Veltman, Nucl. Phys. B **153**, 365 (1979).

[18] G. Passarino and M. J. G. Veltman, Nucl. Phys. B **160**, 151 (1979).

[19] D. M. Pierce, J. A. Bagger, K. T. Matchev and R. j. Zhang, Nucl. Phys. B **491**, 3 (1997).